MNRAS **000**, 1–12 (2016) Preprint 5 July 2016 Compiled using MNRAS LATEX style file v3.0

ExoMol molecular line lists - XVI: The rotation-vibration spectrum of hot H_2S

Ala'a A. A. Azzam[1,2], Jonathan Tennyson[1⋆], Sergei N. Yurchenko[1], Olga V. Naumenko[3]

[1] *Department of Physics and Astronomy, University College London, London WC1E 6BT, UK*
[2] *Department of Physics, The University of Jordan, Queen Rania Street, Amman 11942, Jordan*
[3] *Institute of Atmospheric Optics, Russian Academy of Sciences, Tomsk, Russia*

arXiv:1607.00499v1 [astro-ph.EP] 2 Jul 2016

Accepted XXXX. Received XXXX; in original form XXXX

ABSTRACT

This work presents the AYT2 line list: a comprehensive list of 114 million $^1H_2{}^{32}S$ vibration-rotation transitions computed using an empirically-adjusted potential energy surface and an *ab initio* dipole moment surface. The line list gives complete coverage up to 11000 cm^{-1} (wavelengths longer than 0.91 μm) for temperatures up to 2000 K. Room temperature spectra can be simulated up to 20000 cm^{-1} (0.5 μm) but the predictions at visible wavelengths are less reliable. AYT2 is made available in electronic form as supplementary data to this article and at `www.exomol.com`.

Key words: molecular data; opacity; astronomical data bases: miscellaneous; planets and satellites: atmospheres

1 INTRODUCTION

The investigation of the sulphur chemistry in space is a subject of the active research (Russell & Kivelson 2001; Wakelam et al. 2004; Visscher et al. 2006; Zahnle et al. 2009; Aladro et al. 2011; Hu et al. 2013). In particular Hu et al. (2013) studied the atmospheric composition and the spectra of earth-like exoplanets with sulphur compounds such as hydrogen sulphide (H_2S) and sulphur dioxide (SO_2) using a one-dimensional photochemistry model and associated radiative transfer model to investigate sulphur chemistry in atmospheres ranging from reducing to oxidising. Visscher et al. (2006) used thermochemical equilibrium and kinetic calculations to model sulphur chemistry in giant planets, brown dwarfs, and extrasolar giant planets, and found that H_2S is the dominant S-bearing gas throughout substellar atmospheres and approximately represents the atmospheric sulphur inventory. Therefore, observations of H_2S in these objects should provide a good estimate of their atmospheric sulphur content. H_2S has been, however, ruled out as a potential biosignature in atmospheres of exoplanets according to a biomass-based model study by Seager et al. (2013).

H_2S has long been known in the interstellar medium (Thaddeus et al. 1972) and is important in star-forming (Wakelam et al. 2004; Neufeld, D. A. et al. 2015) and circumstellar (Omont et al. 1993) regions. Aladro et al. (2011) detected H_2S for the first time in galaxy M82, where they studied the chemical complexity towards the central parts of the starburst galaxy, and investigated the role of certain molecules as tracers of the physical processes in the galaxy circumnuclear region. Russell & Kivelson (2001) found evidence for SO_2, SO and H_2S sulphide in Io's exosphere. For Venus, the H_2S composition of the atmosphere at altitudes below 100 km was studied by Von Zahn & Moroz (1985) and de Bergh et al. (2006). Determination of the abundances of gases such as CO, SO_2, OCS, S_2 or H_2S near the surface is important to constrain the oxidation state of the lower atmosphere and surface, and determine the stability of various minerals. Also, measurements at higher altitudes of, for example, SO_3, SO or elemental sulphur, are needed to better understand the sulphur cycle and the chemistry at work below the cloud base. Conversely a recent search for H_2S in volcanic emissions on Mars failed to detect any (Khayat et al. 2015). H_2S is known to be present in comets (Biver et al. 2002) being first detected by Bockelée-Morvan et al. (1991).

On Earth naturally occurring H_2S is associated with volcanic activity (Hoshyaripour et al. 2012). Gaseous H_2S is also detected in a number of other situations including emissions from waste water (Llavador Colomer et al. 2012) and as a by-product of industrial processes (Szabo et al. 2013).

Known experimental absorption spectra of H_2S molecule cover the region from the microwave up to the visible (0.6 μm). Observations include transitions belonging to 59 vibrational bands associated with different 14 polyads

⋆ Email: j.tennyson@ucl.ac.uk

© 2016 The Authors

(Polovtseva et al. 2012), where the polyad number is defined as $n = v_1 + v_2/2 + v_3$, where v_i are standard normal-mode vibrational quantum numbers.

The rotational band has received attention from many experimentalists (Burrus et al. 1953; Huiszoon & Dymanus 1966; Cupp et al. 1968; Miller et al. 1969; Huiszoon 1971; Helminger et al. 1972; Flaud et al. 1983; Burenin et al. 1985; Yamada & Klee 1994; Belov et al. 1995; Azzam et al. 2013; Cazzoli, Gabriele et al. 2014). The first bending vibrational band (ν_2) at 1183 cm^{-1} was studied by Lane et al. (1982), Strow (1983) and Ulenikov et al. (1996a). The two fundamental stretching; symmetric (ν_1) and asymmetric (ν_3) lying at 2615 and 2626 cm^{-1}, respectively, are not isolated but overlapped with strong Coriolis and Fermi resonance interactions. The first triad region ($2\nu_2, \nu_1$, and ν_3) was studied by Gillis & Edwards (1981), the second triad region ($3\nu_2, \nu_1+\nu_2$, and $\nu_2 + \nu_3$) was studied by Snyder & Edwards (1969) and Ulenikov et al. (1996b), while Brown et al. (1998) studied these two triad regions simultaneously. The 4500 – 5600 cm^{-1} spectral region was investigated by Brown et al. (1997). Brown et al. (2004a) and Ulenikov et al. (2005) recorded and analysed the transitions in the region 5700 – 6600 cm^{-1}. In the 7300 – 7900 cm^{-1} region, more than 1550 transitions up to $J = 14$ were recorded and analysed by Ulenikov et al. (2004). The absorption spectrum in the region 8400 – 8900 cm^{-1} was recorded by Brown et al. (2004b). Bykov et al. (1994) recorded and analysed spectra between 2000 to 11 147 cm^{-1}. A number of shorter wavelength regions have been studied, namely, 9540 – 10 000 cm^{-1} by Ding et al. (2003), 10 780 – 11 330 cm^{-1} by Naumenko & Campargue (2001a), 11 930 – 12 300 cm^{-1} by Großkloß et al. (1994) and Flaud et al. (1995), 12 270 – 12 670 cm^{-1} by Vaittinen et al. (1997), near 13 200 cm^{-1} by Campargue & Flaud (1999), 14 100 – 14 400 cm^{-1} by Flaud et al. (1998), and 16 180 – 16 440 cm^{-1} by Naumenko & Campargue (2001b). This situation is summarised in Fig. 1.

All this work has been performed using cool samples, that is below 300 K. The highest recorded value of the rotational quantum number J is 22 in the rotational band region, and the highest predicted value is 27 in the same region. Altogether around 10 000 ro-vibrational energy levels are known from these experiments. The spectroscopic data for the H_2S molecule has been used to populate various spectroscopic databases. Table 1 summarises the contents of the HITRAN-2012 (Rothman et al. 2013), GEISA (Jacquinet-Husson et al. 2011, 2016), W@DIS (Polovtseva et al. 2012), CDMS (Müller et al. 2001, 2005), and JPL (Pickett et al. 1998) databases. All these databases contain data resulting from fitted effective Hamiltonians, apart from W@DIS which contains only measured transitions without intensities. The 2012 release of HITRAN (Rothman et al. 2013) updated HITRAN 2008 (Rothman et al. 2009) using extra rotational data rotational band of H_2S spectrum from Azzam et al. (2013) and the data published in IAO LMS Spectra [spectra.iao.ru].

While absorption spectra of H_2S at elevated temperature have recently been recorded in the ultra-violet by Grosch et al. (2015), we are unaware of any high resolution experimental studies of H_2S infrared spectra at higher than ambient temperature. H_2S cross-sections have been measured up to $T = 50$ C as part of PNNL database (Sharpe et al. 2004).

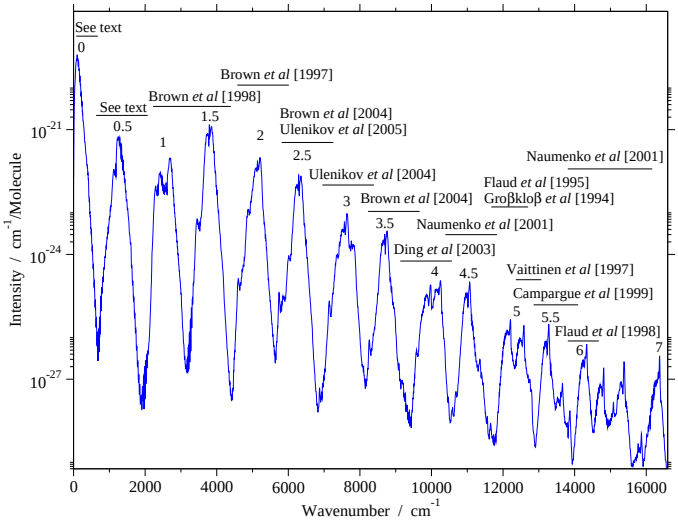

Figure 1. Summary of experimental work on the H_2S absorption spectrum overlayed with our theoretical cross-sections. All spectra were recorded at room temperature. The polyad number of each band is also given.

A number of theoretical studies have considered H_2S. Its ro-vibrational spectrum was calculated by Senekowitsch et al. (1989), Tarczay et al. (2001) and Tyuterev et al. (2004). In the work of Senekowitsch et al. (1989), the room temperature absorption ro-vibrational spectrum of H_2S was calculated variationally for the pure rotational and ν_2, $2\nu_2$, ν_1, and ν_3 transitions from $J = 0$ to 13, where the full account of the anharmonicity effects and ro-vibration couplings were considered. Senekowitsch et al. (1989) calculated the vibrational band origins of the fundamental transitions with accuracy better than 10 cm^{-1}, and the ro-vibrational transitions to within a few tenths of a cm^{-1} for low J's and up to a few cm^{-1} for high J's; their work was also extended to deuterated isotopologues (Miller et al. 1990). The anomalies in the spectral intensity for this molecule were obtained qualitatively. Tarczay et al. (2001) calculated the vibrational band origins of $H_2{}^{32}S$ with accuracy of 29 cm^{-1} up to 14 300 cm^{-1}, and the rotational transitions of the ground vibrational state for $J = 17$ with deviations from the experimental values from 2 to 10 cm^{-1}. Tyuterev et al. (2004) used a spectroscopically-determined potential energy surface to compute the spectrum in the interval 0 – 8000 cm^{-1}, for J up to 18 and with and intensity cut-off $\leq$ 10^{-27} cm^{-1}/(molecule×cm^{-2}); they reported calculated transitions to be better than 0.01 cm^{-1} for the line positions and 1-3% in the intensities for the strong and medium lines and to ∼10% for the weak lines for room temperature conditions. Very recently Carvajal & Lemus (2015) explored the use of ladder operators to study the vibrational spectrum of this system.

Remote detection of H_2S relies on well-characterised laboratory spectra. At higher temperatures the resulting list of transitions becomes very extensive and is best calculated using a robust theoretical model (Tennyson 2012). The ExoMol project (Tennyson & Yurchenko 2012) aims to provide molecular line lists for exoplanet and other atmospheres with a particular emphasis on hot species. In this work we present

Table 1. Summary for the H_2S spectral data available in different databases.

Database	isotopologue	Bands #	Transitions #	Wavenumber$_{min}$ (cm^{-1})	Wavenumber$_{max}$ (cm^{-1})
HITRAN 2012	$H_2{}^{32}S$	49	36561	2	11330
	$H_2{}^{33}S$	19	6322	5	11072
	$H_2{}^{34}S$	24	11352	5	11227
GEISA	$H_2{}^{32}S$	14	12330	2	4257
	$H_2{}^{33}S$	8	3564	5	4098
	$H_2{}^{34}S$	8	4894	5	4171
W@DIS	$H_2{}^{32}S$	59	34148	1	16437
CDMS	$H_2{}^{32}S$	1	1501	1	554
	$H_2{}^{33}S$	1	4759	1	402
	$H_2{}^{34}S$	1	990	1	444
JPL	$H_2{}^{32}S$	1	1525	1	333

a comprehensive, hot linelist of vibration-rotation transitions of $^1H_2{}^{32}S$. This line list should be appropriate for temperatures up to 2000 K. The methodology used, which is discussed in the following section, closely follows that used to generate comprehensive hot line lists for triatomic species such as water (Barber et al. 2006; Kyuberis et al. 2016) and, recently, SO_2 (Underwood et al. 2016). Section 3 presents our line list computations. Results and comparisons are given in section 4. Section 5 gives our conclusions.

2 THEORETICAL METHOD

In order to compute a line list for H_2S three things are required (Lodi & Tennyson 2010): a suitable potential energy surface (PES), dipole moment surfaces (DMS), and a nuclear motion program. Each of these are considered in turn below.

2.1 Potential Energy Surfaces

Four PESs were tested. Our starting point was an *ab initio* PES constructed using the CCSD(T)/aug-cc-pV(Q+d)Z level of theory as implemented in Molpro (Werner et al. 2012). This surface was fitted to the function form given by Tyuterev et al. (2001) using 1200 geometries covering the energy range up to 40 000 cm^{-1} above equilibrium. The surface was then refined by fitting it to the available experimental values of H_2S for $J \leq 6$ covering the energy range up to 16 500 cm^{-1} with a root-mean-square (rms) error of 0.03 cm^{-1} for the fit. We will call this surface PES-Y. This surface was tested by calculating the energy levels for $J = 0$, 1, 2, 5 and 10, and comparing the results with experimental energy levels.

The second PES, PES-T, was constructed by Tyuterev et al. (2001), using a dataset of then-available experimentally determined H_2S energy levels. This surface was obtained by the simultaneous fit of a large sample of high-resolution ro-vibrational data, using an extensive set of more than 12 000 experimental ro-vibrational transitions for 7 isotopologues of H_2S. This surface is the most accurate available empirically-determined, PES. However, using the published parameters of PES-T and calculating the ro-vibrational energy levels, we found some problems. Tyuterev *et al.* used Dvr3d (Tennyson et al. 2004) to confirm the convergence of the basis set used in their work for high vibrational states. First, calculating the vibrational energy levels using PES-T with the parameters suggested for Dvr3d by Tyuterev *et al.* ($r_e = 2.75$, $D_e = 0.1$, $\omega_e = 0.01$, all in a.u., NPNT2 = 35 and NALF = 98), and then comparing these calculated energy values with the experimental vibrational energy levels taken from Tyuterev et al. (2001), we could not reproduce the values for the vibrational energy levels as published by Tyuterev *et al.*. Second, testing PES-T for convergence shows that increasing the number of the radial points, NPTN2, some of the energy levels become negative. Graphical investigations showed that this surface develops a hole when the atoms all lie close together. This problem was solved by considering the coefficients up to the quadratic order and ignoring the coefficients with the higher orders in the refining function for the energies above 50 000 cm^{-1}. The modified PES-T was used to calculate the vibrational energy levels again. A further problem is that we found Tyuterev *et al.*'s vibrational basis set is not converged above 9000 cm^{-1}.

PES-T was further refined using updated experimental levels lying up to 17 000 cm^{-1}; 71 parameters were fitted in two different refinements: (1) using experimental energy levels with $J = 0$, 1, 2 and 5; (2) using experimental energy levels with $J \leq 6$. The resulting two PESs will be referred to as PES-Y0125 and PES-Y0-6, respectively. Convergence tests were performed also for these new refined surfaces by calculating ro-vibrational energy levels for $J = 0$, 1, 2, 5 and 10, and comparing the calculated values with the available experimental data. PES-Y0125 gives better results than PES-Y0-6.

PES-Y0125 predicts experimentally known energy levels with $J \leq 10$ with a standard deviation of 0.11 cm^{-1} compared to 0.23 cm^{-1} using PES-T (using our parameters for Dvr3d). Note that Tyuterev *et al.* claimed that their PES predicted the experimentally known levels with $J \leq 15$ with a standard deviation of 0.03 cm^{-1} for all isotopologues. Table 3 shows the standard deviations for the calculated ro-vibrational energy levels up to 17 000 cm^{-1} using PES-T and PES-Y0125 for $J = 0$, 1, 2, 5 and 10. These calculations show that using PES-Y0125, around 7% of the ro-vibrational energy level with $J \leq 5$ values have errors more than 0.25 cm^{-1}. All of these levels lie above 12 450 cm^{-1}. This proportion increases with J so that 26% of levels are more than 0.25 cm^{-1} away from the observed $J = 10$ levels, all of them above 8600 cm^{-1}. PES-Y0125 was adopted for this study.

Table 2. Comparison between the experimental and the calculated vibrational levels in cm^{-1}. Columns 1 and 2 give quantum numbers in normal and local modes. Column 3 gives observed vibrational bands origins, see Tyuterev et al. (2001); column 4 gives the residuals of these bands origins published by Tyuterev et al. (2001); column 5 gives the residuals of the bands origins computed using PES-T with the Dvr3d parameters suggested by Tyuterev et al. (2001); column 6 gives residuals of the bands origins computed using PES-Y0125 and our parameters for Dvr3d.

Normal ($\nu_1\nu_2\nu_3$)	Local [n_1 $n_3^{\pm}$,b]	Obs.	Obs.-Calc. 4	5	6
(010)	[00$^+$,1]	1182.58	-0.01	-0.01	0.02
(020)	[00$^+$,2]	2353.96	0.00	-0.01	-0.02
(100)	[10$^+$,0]	2614.41	-0.02	-0.01	0.06
(030)	[00$^+$,3]	3513.79	0.00	0.00	-0.13
(110)	[10$^+$,1]	3779.17	0.00	0.00	-0.11
(040)	[00$^+$,4]	4661.68	-0.01	0.00	-0.35
(120)	[10$^+$,2]	4932.70	0.01	0.01	-0.16
(200)	[20$^+$,0]	5144.99	-0.01	0.02	0.07
(002)	[11$^+$,0]	5243.10	-0.02	-0.01	0.05
(050)	[00$^+$,5]	5797.24	0.01	0.01	-0.69
(130)	[10$^+$,3]	6074.58	-0.04	-0.04	-0.23
(210)	[20$^+$,1]	6288.15	0.04	0.07	0.05
(102)	[30$^+$,0]	7576.38	-0.03	0.04	0.02
(300)	[21$^+$,0]	7752.26	-0.01	0.02	0.15
(112)	[30$^+$,1]	8697.14	-0.01	0.06	0.08
(202)	[40$^+$,0]	9911.02	0.00	0.18	0.04
(400)	[31$^+$,0]	10188.30	-0.01	0.06	0.12
(212)	[40$^+$,1]	11008.68	-0.05	0.13	-0.02
(302)	[50$^+$,0]	12149.46	0.04	0.40	0.21
(104)	[41$^+$,0]	12524.63	0.01	0.19	0.07
(312)	[50$^+$,1]	13222.77	0.05	0.42	-0.22
(322)	[50$^+$,2]	14284.71	0.02	0.42	-0.74
(402)	[60$^+$,0]	14291.12	0.03	0.66	0.58

Table 3. Standard deviation values of the ro-vibrational energy levels up to 17 000 cm^{-1} for J = 0, 1, 2, 5 and 10.

	Standard deviation (cm^{-1})	
J	PES-Y0125	PES-T
0	0.19	0.24
1	0.06	0.21
2	0.07	0.21
5	0.07	0.23
10	0.19	0.24

2.2 Dipole Moment Surfaces

The preferred method of generating accurate intensities is to use *ab initio* DMS (Lynas-Gray et al. 1995; Tennyson 2014; Polyansky et al. 2015). However H_2S intensities are known to be particularly difficult to reproduce since they display a number of anomalies. For example, the observed intensity of all the fundamental bands of H_2S are two-to-three orders of magnitude weaker than those in similar triatomics such as H_2O and H_2Se, and are also much weaker than those of combination bands ($\nu_1+\nu_2$, $\nu_2+\nu_3$ and $\nu_1+\nu_3$) (Brown et al. 1998). In particular the usually strong asymmetric stretch fundamental band ν_3 is even weaker than the $2\nu_2$ bending overtone. Furthermore all fundamental bands show intensity anomalies in their rotational distributions (Brown et al. 1998; Gillis & Edwards 1981; Strow 1983). For the ν_3 band, some 'forbidden' $\Delta K_a = \pm 2$ transitions are actually more intense than the corresponding 'allowed' $\Delta K_a = 0$ transitions (Brown et al. 1998). Reproducing this behaviour *ab initio* therefore represents a considerable challenge. *Ab initio* DMS have been calculated for H_2S by Senekowitsch et al. (1989), by Cours, Tyuterev and co-workers (Cours et al. 2002, 2000; Henon et al. 2003) and us (Azzam et al. 2015).

In this work we use the ALYT2 DMS of Azzam et al. (2015) which uses a CCSD(T)/aug-cc-pV(6+d)Z level of theory supplemented by a core-correlation/relativistic corrective surface obtained at the CCSD[T]/aug-cc-pCV5Z-DK level. The intensities computed with this surface agree to within 10 % when compared with directly measured experimental data. Further details can be found in Azzam et al. (2015).

Table 4. Input parameters for DVR3DRJZ and ROTLEV3B modules of DVR3D (Tennyson et al. 2004).

Parameter	Value	Description
DVR3DRJZ		
NPNT2	40	No. of radial DVR points (Gauss-Laguerre)
NALF	48	No. of angular DVR points (Gauss-Legendre)
NEVAL	2000	No. of eigenvalues/eigenvectors required
MAX3D	6000	Dimension of final vibrational Hamiltonian
XMASS (S)	31.972071 Da	Mass of sulphur atom
XMASS (H)	1.007825 Da	Mass of oxygen atom
r_e	3.8 a_0	Morse parameter (radial basis function)
D_e	0.4 E_h	Morse parameter (radial basis function)
ω_e	0.005 a.u.	Morse parameter (radial basis function)
ROTLEV3B		
NVIB	1400	No. of vib. functions used for each K

2.3 Nuclear motion calculations

Ro-vibrational spectra were computed using the Dvr3dr program suite (Tennyson et al. 2004) in Radau coordinates and a bisector embedding. Analysis showed that the published version Dvr3dr used a very significant amount of time constructing the final Hamiltonian matrix in module rotlev3b. rotlev3b uses vibrational functions generated in the first step of the calculation (Tennyson & Sutcliffe 1986) to provide basis functions for the full ro-vibrational calculation performed by rotlev3b. For high J calculations this algorithm involves transforming large numbers of off-diagonal matrix elements to the vibrational basis set representation, see Eq. (31) in Tennyson & Sutcliffe (1992). This step can be refactored as two successive summations rather than a double summation. The savings in doing this proved to be very significant, so much so that computing the hot ATY2 linelist was actually much quicker than generating the original (unpublished) small ATY1 room temperature line list.

Considerable care was taken to ensure convergence of the final calculations, see Azzam (2013) for details. Table 4 gives the parameters used in the final calculation which is sufficient to converge all energy levels consider to about 0.2 cm^{-1}, and very much better than this for the vast majority of them.

3 LINE LIST CALCULATIONS

The calculations for the ATY2 were performed using 16 processors on the machine Amun which are Intel(R) Xeon(R) CPU E7340 @ 2.40GHz. All states with $J \leq 40$ lying up to 21 000 cm^{-1} above the vibrational ground state were included. Einstein A-coefficients were generated by considering all transitions involving a lower state below 10 000 cm^{-1}. As discussed below this means that the AYT2 line list is complete at higher temperatures for transition wavenumbers up to 11 000 cm^{-1}. At lower temperatures it is complete to higher wavenumbers, about 20 000 cm^{-1} at 296 K. The full

Table 5. Extract from the state file for H_2S. The full table is available from http://cdsarc.u-strasbg.fr/cgi-bin/VizieR?-source=J/MNRAS/xxx/yy.

i	$\tilde{E}$	g	J	τ	Γ	K_a	K_c	ν_1	ν_2	ν_3
1	0.000000	1	0	inf	A1	0	0	0	0	0
2	1182.569618	1	0	2.2209E+01	A1	0	0	0	1	0
3	2353.907317	1	0	9.9513E+00	A1	0	0	0	2	0
4	2614.394829	1	0	1.5263E+01	A1	0	0	1	0	0
5	3513.705072	1	0	5.1249E+00	A1	0	0	0	3	0
6	3779.189348	1	0	1.0827E+00	A1	0	0	1	1	0
7	4661.605794	1	0	2.7037E+00	A1	0	0	0	4	0
8	4932.688937	1	0	5.7855E-01	A1	0	0	1	2	0
9	5145.031868	1	0	2.2070E+00	A1	0	0	2	0	0
10	5243.158956	1	0	2.7018E+00	A1	0	0	0	0	2
11	5797.207552	1	0	1.4956E+00	A1	0	0	0	5	0
12	6074.566059	1	0	3.9968E-01	A1	0	0	1	3	0
13	6288.134723	1	0	4.0625E-01	A1	0	0	2	1	0
14	6385.320930	1	0	3.4910E-01	A1	0	0	0	1	2
15	6920.081316	1	0	8.8597E-01	A1	0	0	0	6	0
16	7204.435162	1	0	3.0530E-01	A1	0	0	1	4	0

i: State counting number.
$\tilde{E}$: State energy in cm^{-1}.
g: State degeneracy.
J: Total angular momentum
τ: State lifetime in s^{-1}, see Tennyson et al. (2016b).
Γ: Symmetry.
ν_1: Symmetric stretch quantum number.
ν_2: Bending quantum number.
ν_3: Asymmetric stretch quantum number.
K_a: Asymmetric top quantum number.
K_c: Asymmetric top quantum number.

Table 6. Extract from the transitions file for H_2S. The full table is available from http://cdsarc.u-strasbg.fr/cgi-bin/VizieR?-source=J/MNRAS/xxx/yy.

f	i	A_{fi}
54311	54310	8.2902e-04
96461	90862	7.0642e-10
95160	95159	2.9992e-04
182973	182972	6.2635e-13
66321	66320	8.0872e-08
63788	54387	1.4876e-09
166858	166857	4.1485e-09
66292	66291	1.4730e-07
118595	119927	3.3674e-08
12533	9738	2.2129e-02
67918	67917	2.2181e-02
19633	14097	7.6778e-05
44469	44468	1.8778e-12
41993	41992	2.5145e-06
64167	58776	8.1489e-13
49157	41344	3.7880e-01
44472	39869	3.7880e-01
183309	183308	1.2889e-11
49527	49526	3.3570e-10
86003	80100	9.6741e-12
31768	31767	1.8568e-04

f: Upper state counting number;
i: Lower state counting number;
A_{fi}: Einstein-A coefficient in s^{-1}.

line list has 113 945 193 lines sorted by frequency and split into 20 files in 1000 cm^{-1} portions.

Table 5 gives a portion of the H_2S states file. DVR3D does not provide approximate quantum numbers: K_a, K_c or the normal mode vibrational labels ν_1, ν_2 and ν_3. Lower-lying levels were checked and assigned quantum numbers on the basis of comparison with effective Hamiltonians. For higher levels below about 16 000 cm^{-1}, labels were taken from calculations performed with TROVE (Yurchenko et al. 2007) and used the correlation between DVR3D and TROVE. The higher stretching states of H_2S are actually better represented by local mode (Jensen 2012) rather than normal mode quantum numbers. However, since there is a one-to-one correspondence between these two representations for XH_2 molecules (Carleer et al. 1999), we simply use the normal mode representation. We note that these quantum numbers are approximate and may be updated in future as better estimates become available. The table also includes a column which gives the calculated radiative decay lifetime for each state. This is a new feature in the ExoMol file structures (Tennyson et al. 2016a). Table 6 gives a portion of the ATY2 transitions file.

3.1 Room temperature comparisons

The accuracy of the calculated spectrum can be checked by comparing the transition positions and intensities with their counterparts in the literature and the databases. The only available experimental data for H_2S spectrum is at room temperature (T = 296 K), so we judge the accuracy of our calculations using the spectrum calculated at this temperature. This is not always straightforward for two reasons. First, in order to compare spectra in detail, full assignments are required for the transitions and this is not the case for the calculated transitions using Dvr3d. Second, our dipole study (Azzam et al. 2015) showed that agreement between our calculations and experimentally measured transitions is much better than with transitions which are the result of (effective Hamiltonian) predictions. As a result, during the comparison, we distinguish between the experimental and predicted transitions.

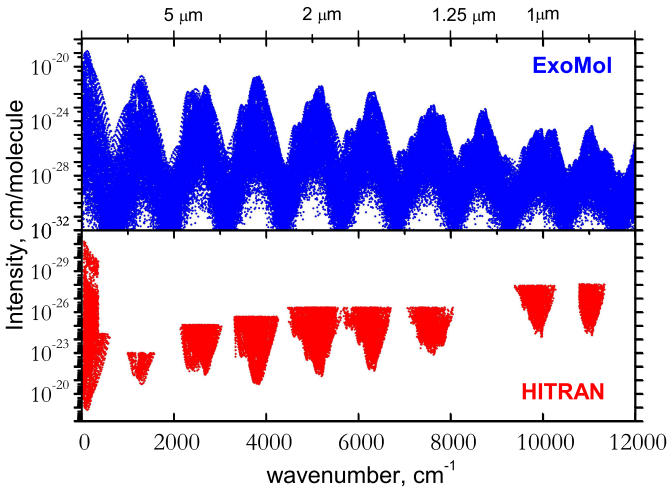

Figure 2. A T = 296 K absorption stick spectrum of H_2S: Comparison with HITRAN 2012.

As a preliminary comparison, Fig. 2 gives a general idea about the number of transitions available in HITRAN 2012 (Rothman et al. 2013) compared to the number of transitions calculated in this work at room temperature. Also, Figs. 3 and 4 give a general idea about the accuracy of our calculated line list (ATY2) compared to the data in these databases; more detailed comparisons are presented in the following subsections.

The data available in HITRAN 2012 for $H_2{}^{32}S$ comprise 36 533 transitions in the spectral region 2- 11330 cm^{-1} and covers J values up to 30 and cut-off intensity of the order of 10^{-32} $cm^{-1}/(molecule \times cm^{-2})$ at 296 K. Our compar-

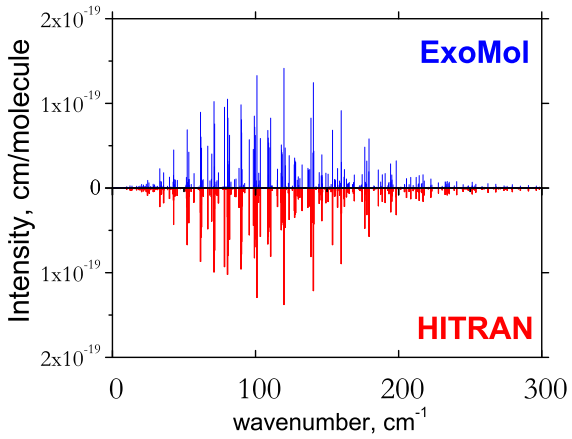

Figure 3. A calculated rotational band compared to that from the HITRAN database at $T = 296$ K.

isons prioritise actual measured line positions and intensities, which we identified from the data given in HITRAN using additional information provided by the IS WADIS (wadis.saga.iao.ru) database. A summary of the comparison between our calculations and the data in HITRAN database for every polyad region is presented in Tables 7, 8 and 9.

3.1.1 HITRAN database: 0–4200 cm^{-1}

HITRAN 2012 contains around 14 700 transitions in the 0–4250 cm^{-1} spectral region with an intensity cut-off of the order of 10^{-32} below 360 cm^{-1} and 10^{-26} cm^{-1}/(molecule×cm^{-2}) above 360 cm^{-1}. Of all data provided by the HITRAN 2012 in this region, only around 10 700 transitions with positions either measured or accurately determined from the upper and lower experimental energy levels are included in our comparison. In addition, about 550 simulated transitions of the 010–000 band between 1000 and 1570 cm^{-1} were also used, as no other data are available in HITRAN 2012 for this region. It should be noted that all intensities provided by the HITRAN below 4250 cm^{-1} are calculated values. Figure 5 shows the differences between ATY2 and HITRAN2012 in this region for both transition frequencies and intensities. A summary of the comparison between our calculations and the HITRAN data for polyad 0 to 1.5 is presented in Tables 7-8.

For the pure rotational region 0-360 cm^{-1} (000 - 000 and 010-010 transitions), the standard or rms deviation between the calculated and measured (Flaud et al. 1983; Azzam et al. 2013) positions up to $J = 26$ is 0.016 cm^{-1} for 1815 observed lines with maximum absolute deviation of 0.094 cm^{-1}. All the intensities in this region are calculated using the permanent dipole moment. Both sets of calculated intensities provided by HITRAN and variational agree very well with an rms of 5.7% and average ratio of 1.04.

Positions of the 010–000 band (polyad 0.5) in HITRAN were simulated based on the spectroscopic parameters reported by Lane et al. (1982) and then normalized to the measured values of Strow (1983). Comparison with AYT2 yields an rms and maximal deviations for line positions of 0.049 and 0.258 cm^{-1}. Variational intensities for the 010–000 band

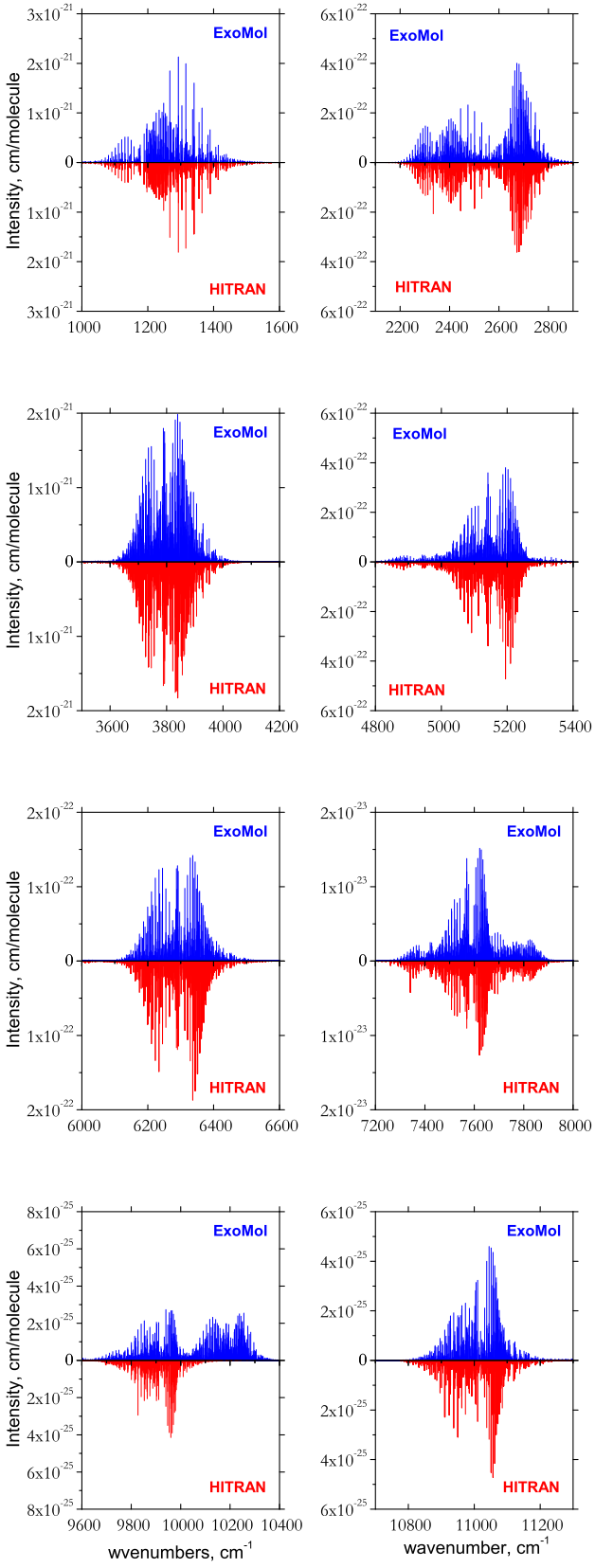

Figure 4. Calculated spectrum at $T = 296$ K compared to that from the HITRAN database for the polyads (top left to bottom right) 0.5, 1, 1.5, 2, 2.5, 3, 4 and 4.5.

differ significantly from a simulation adopted in HITRAN with an rms deviation of 30%. Measured intensities of 103 lines of the 010–000 band reported by Strow (1983) , deviate from variational values within an rms of 23%. The integrated variational intensity of the 010–000 band is about 17% larger than that estimated from HITRAN. This is in agreement with tests for $J \leq 5$ made previously by Azzam et al. (2015).

For the 2140-4250 cm^{-1} spectral region our comparison was limited to 7505 'empirical' transitions. Similar rms and maximum deviations around 0.07 and 0.36 cm^{-1}, respectively, have been obtained between 'empirical' and calculated positions for polyads 1 and 1.5. In this comparison we used corrected set of the transition positions above 2000 cm^{-1} which corresponds to the original data of Brown et al. (1998). These data are available in the 2015 release of the GEISA-2015 database (Jacquinet-Husson et al. 2016).

Above 2200 cm^{-1} the transition intensities adopted in HITRAN are taken from an effective Hamiltonian based on about 1100 accurate (within 2-5%) measured intensities reported by Brown et al. (1998). Comparison of the AYT2 intensities with the HITRAN data and accurate measured values is summarized in Table 7 and is illustrated on Fig.5. Reasonable agreement between the measured and variational intensities within an rms of 8%, is achieved, while the predicted HITRAN intensities deviate from the AYT2 predictions by about 16-18% .

3.1.2 HITRAN database: 4400-8000 cm^{-1}

The H_2S transitions in the 4400-8000 cm^{-1} region represent measured positions and intensities which are augmented with 'empirical' transitions generated from experimental energy levels and intensities predicted using an effective Hamiltonian. Of 16 284 transitions included in HITRAN2012, 11 277 correspond to observed data. It should be noted that majority of the measured intensities are of low accuracy, often derived from a peak absorption. However, for about 2500 transitions between 4580 and 6575 cm^{-1}, accurate intensities are provided.

Only observed data were used in comparison with variational calculation. A summary of this comparison is given in Table 8 and Fig. 6. The observed position are reproduced with an rms of 0.08 cm^{-1} (polyad 2.5) and 0.13 cm^{-1} (polyads 2 and 3) with maximal deviations not exceeding 0.6 cm^{-1}.

Intensity comparisons are not so straightforward with strongly distorted ratios between observed and AYT2 intensitions for individual transitions. Sometimes this disagreement is due to missing additional lines, or due to incorrect assignment, sometimes the experimental line is a superposition with another H_2S isotopologue, removed from the list. There is also the possibility of increased errors in the AYT2 intensities for individual vibrational bands, due to problems with the DMS, or for individual transitions, due to perturbations (Lodi & Tennyson 2012; Zak et al. 2016). The distribution of intensity ratios was examined for every polyad, and the suitable upper and lower limits chosen which included 91 - 95% of the lines; these were used to determine the rms deviations presented in Table 8.

The best intensity agreement, with an rms of 6.9%, was obtained for accurate 1423 experimental intensities for

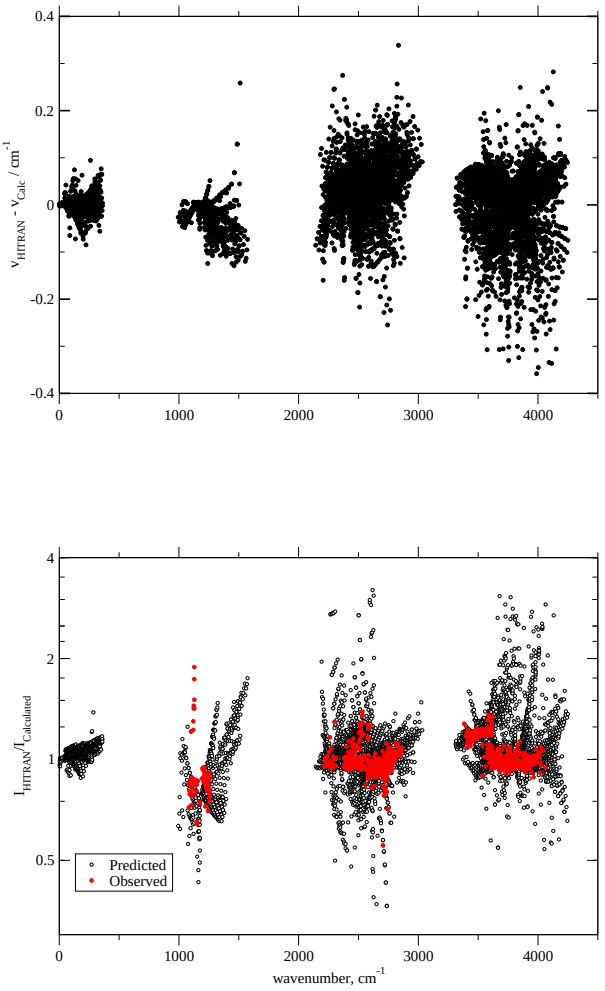

Figure 5. Differences in line positions (upper) and transition intensities (lower) compared to data available in HITRAN below 4000 cm^{-1}. The measured and predicted lines in this database are considered separately.

polyad 2, while the rms for all observed lines for this polyad was about 25%. At the same time, intensities of transitions belonging to polyad 2.5 deviated from their AYT2 analogs, see Table 8 and Fig.6, both for approximate and accurate measured data: of 1084 accurate intensities only 1019 could be reproduced with an rms of 14%. We note that our calculation appear to overestimate the strength of the $5\nu_2$ band, which lies at about 5800 cm^{-1}, by approximately a factor of 2. This is almost certainly caused by residual problems with DMS of Azzam et al. (2015).

3.1.3 HITRAN database: 9500-11300 cm^{-1}

The HITRAN2012 data for H_2S in this region comprises the measurements of Naumenko & Campargue (2001a) and Naumenko & Campargue (2001b) augmented by the calculated lines with 'empirical' positions and intensities predicted on the basis of and effective Hamiltonian model. Of 5605

Table 7. Comparison between the calculated transitions and the data available in HITRAN for the polyad regions 0 and 0.5. σ is the standard deviation. Absolute intensities are in $cm^{-1}/(molecule \times cm^{-2})$ (powers of ten in parenthesis) and errors are all relative; the frequency errors are absolute errors. The HITRAN data are divided between directly measured and predicted from effective Hamiltonians.

Polyad	Frequency		Intensity		
		Measured		Predicted	Measured
0	Spectral Range	3 – 360 cm^{-1}	Intensity Range	1.53(-26) – 9.91(-20)	
	J range	1 – 26	Average ratio	1.04	
	K_a range	0 – 17	σ	5.7 %	
	σ	0.016 cm^{-1}	Min. ratio	0.88	
	Max. deviation	0.094 cm^{-1}	Max. ratio	1.38	
	Total # lines	1185		1185	
0.5	Spectral range	994 – 1573 cm^{-1}	Intensity Range	9.10(-24) – 1.81(-21)	1.52(-24) – 8.34(-21)
	J range	1 – 16	Average ratio	0.93	0.90
	K_a range	0 – 14	σ	30 %	23 %
	σ	0.016 cm^{-1}	Min. ratio	0.43	0.64
	Max. deviation	0.094 cm^{-1}	Max. ratio	1.75	1.88
	Total # lines	551		551	103

Table 8. Comparison between the calculated transitions and the data available in HITRAN for the polyad regions 1 and 1.5. σ is the standard deviation. Absolute intensities are in $cm^{-1}/(molecule \times cm^{-2})$ (powers of ten in parenthesis) and errors are all relative; the frequency errors are absolute errors. The HITRAN data are divided between directly measured and predicted from effective Hamiltonians.

Polyad	Frequency		Intensity		
		Empirical		Predicted	Measured
1	Spectral Range	2142 – 3034 cm^{-1}	Intensity Range	8.07(-26) – 3.61(-22)	5.90(-25) – 2.73(-22)
	J range	0 – 20	Average ratio	1.03	0.99
	K_a range	0 – 14	σ	17.9%	8.2 %
	σ	0.070 cm^{-1}	Min. ratio	0.36	0.55
	Max. deviation	0.338 cm^{-1}	Max. ratio	3.18	1.39
	Total # lines	3453		3413	568
1.5	Spectral range	3312 – 4250 cm^{-1}	Intensity Range	2.04(-26) – 1.83(-21)	4.89(-25) – 1.77(-21)
	J range	0 – 20	Average ratio	1.09	1.02
	K_a range	0 – 15	σ	15.6%	7.5 %
	σ	0.072 cm^{-1}	Min. ratio	0.54	0.88
	Max. deviation	0.358 cm^{-1}	Max. ratio	3.06	1.35
	Total # lines	4050		4026	526

transitions, only 2835 have measured positions and intensities. Experimental intensities were estimated to be accurate to 25-30% on average and up to 100% for the weakest lines in polyad 4 region, and as 15% for strong and medium intensity lines and up to 50% for weakest lines for polyad 4.5.

Again only measured transitions were used in the comparison. Table 9 summarizes the results of the analysis which are shown graphically in Fig. 7. Agreement between the observed and AYT2 line positions was found to be quite satisfactory with an rms of 0.086 and 0.138 cm^{-1} for polyad 4.5 and 4, respectively, while the maximal deviation does not exceed 0.67 cm^{-1} for both polyads. However, the intensities agree less well than for the lower polyads with an rms of 54-56% when about 90% of lines were compared. Much larger deviations in intensity ratios (up to 2 orders of magnitude) were also encountered. They may be caused by the low accuracy of the experimental intensities, incomplete or incorrect assignments, or by distortion of the calculated values. It seems that calculated intensities of transitions involving the upper states in the local mode limit are strongly sensitive to the details of the PES, and can change significantly for its different versions.

In general, our calculations agree well with the measured transition intensities where we find the difference of up to about a factor of 3 while much larger differences sometimes up to two-three orders of magnitudes appear for results derived from effective Hamiltonians (not shown). This analysis suggests that there are problems with the effective Hamiltonian extrapolation; this problem will be analysed elsewhere.

Our calculated spectrum at room temperature contains around 620 000 transitions up to $J = 40$ below 12 000 cm^{-1} with the intensity cut-off 10^{-31} $cm^{-1}/(molecule \times cm^{-2})$ comparing to 36 600 transitions in HITRAN 2012. This spectrum has a standard deviation for the transition positions of about 0.072 cm^{-1} for 94% of the 20 513 most accurate measured lines below 8000 cm^{-1} (see Tables 7-9). The standard deviation of the ratios of the transition intensities in HITRAN 2012 to the calculated intensities is 10% with an average ratio of 1.02 for 76% of lines considered, provided that the less accurate 010–000 transition intensities were excluded from consideration.

Table 9. Comparison between the calculated transitions and the data available in HITRAN for the polyad regions 2 and 2.5. σ is the standard deviation. Absolute intensities are in $cm^{-1}/(molecule \times cm^{-2})$ (powers of ten in parenthesis) and errors are all relative; the frequency errors are absolute errors. The HITRAN data are divided between accurately and approximately measured.

Polyad	Frequency		Intensity		
		Measured		Approx. measured	Measured
2	Spectral range	4486 – 5595 cm^{-1}	Intensity Range	1.88(-26) – 4.72(-22)	4.26(-26) – 4.09(-22)
	J range	0 – 20	Average ratio	1.08	1.01
	K_a range	0 – 14	σ	24.8%	6.9 %
	σ	0.127 cm^{-1}	Min. ratio	0.50	0.76
	Max. deviation	0.524 cm^{-1}	Max. ratio	3.00	1.38
	Total # lines	5617		5165	1423
2.5	Spectral range	5688 – 6653 cm^{-1}	Intensity Range	1.60(-26) – 1.87(-22)	2.11(-26) – 1.87(-22)
	J range	0 – 18	Average ratio	1.12	1.05
	K_a range	0 – 14	σ	32.3%	14.0 %
	σ	0.078 cm^{-1}	Min. ratio	0.40	0.71
	Max. deviation	0.293 cm^{-1}	Max. ratio	3.00	1.50
	Total # lines	3153		3014	1019
3	Spectral range	7096 – 7995 cm^{-1}	Intensity Range	1.63(-26) – 1.26(-23)	
	J range	0 – 17	Average ratio	0.99	
	K_a range	0 – 10	σ	33.8%	
	σ	0.129 cm^{-1}	Min. ratio	0.50	
	Max. deviation	0.358 cm^{-1}	Max. ratio	3.00	
	Total # lines	2504		2327	
4	Spectral range	9541 – 10001 cm^{-1}	Intensity Range	2.98(-28) – 6.09(-25)	
	J range	0 – 17	Average ratio	1.48	
	K_a range	0 – 11	σ	54%	
	σ	0.138 cm^{-1}	Min. ratio	0.25	
	Max. deviation	0.670 cm^{-1}	Max. ratio	3.95	
	Total # lines	1716		1568	
4.5	Spectral range	10790 – 11298 cm^{-1}	Intensity Range	2.67(-28) – 4.72(-25)	
	J range	0 – 19	Average ratio	1.48	
	K_a range	0 – 11	σ	56%	
	σ	0.086 cm^{-1}	Min. ratio	0.27	
	Max. deviation	0.580 cm^{-1}	Max. ratio	2.86	
	Total # lines	1093		1015	

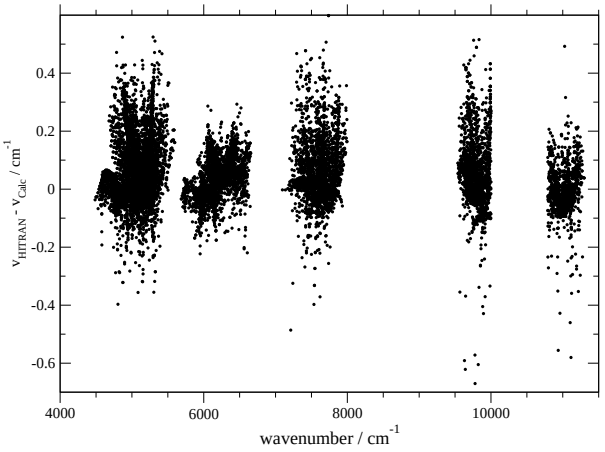

Figure 6. Differences in line positions comparing to actual observed data included in HTRAN2012.

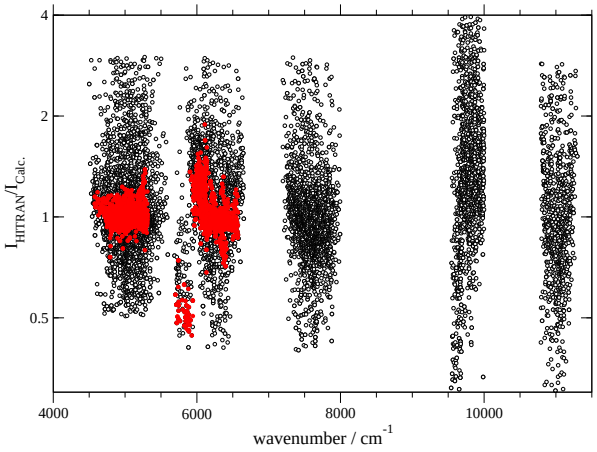

Figure 7. Errors in transition intensities comparing to actual observed data included in HTRAN2012; intensities for which the measurements are accurate are highlighted.

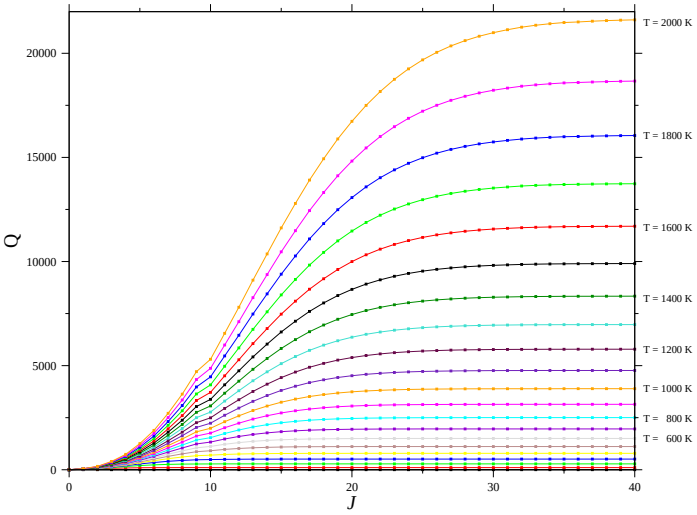

Figure 8. Partition functions convergence curves.

4 PARTITION FUNCTION AND LIFETIMES

The partition function value (Q) of a molecule at temperature (T) is given by

$$Q(T) = \sum_J \sum_i g_i(2J+1) \exp\left(-\frac{c_2 E_i^{(J)}}{T}\right), \qquad (1)$$

where g is the nuclear statistical weight which is 1 or 3 for para or ortho states of $H_2{}^{32}S$ in the convention adopted by HITRAN and ExoMol; $E_i^{(J)}$ is the ro-vibrational energy for a given J value, and c_2 is the second radiation constant. The summation in this equation should be performed over all ro-vibrational energy levels with or at least until the value of Q converges. Figure 8 shows how Q converges with J at different temperatures up to 2000 K. Table 10 presents $H_2{}^{32}S$ Q values at different temperatures in comparison with the values from the HITRAN, the JPL (Pickett et al. 1998), and the CDMS databases.

The lifetimes of H_2S were computed using the Einstein A coefficients from the ATY2 linelist following the methodology laid out by Tennyson et al. (2016a). Results are summarisd in Fig. 9; we note that the lifetimes are much more regular as function of changes in quantum numbers than those computed by (Tennyson et al. 2016a) for water.

5 HOT SPECTRA

Fig. 10 shows the calculated spectra at different temperatures. This figure shows how the weak transitions at low temperatures become stronger at higher temperatures. The spectrum at 2000 K contains 46 million transitions up to 12 000 cm^{-1}, with $J \leq 40$ with intensities below 10^{-31} cm^{-1}/(molecule×cm^{-2}). Transition positions do not change with temperature unlike transition intensities which are temperature dependent due to the $e^{-E_{\rm low}/kT}$ Boltzmann factor. The ATY2 line list can also be used to simulate room temperature spectra up to 20000 cm^{-1}; however, our calculations are less accurate at visible wavelengths,

No experimental line intensities of H_2S can be found to compare our calculations with, neither experimental nor theoretical with temperatures higher than 296 K. This made our line list as the first available source of data for $H_2{}^{32}S$ spectrum at temperatures higher than the room temperature, thus, opening the door for probability of identifying $H_2{}^{32}S$ transitions in exoplanet and brown dwarfs atmospheres. This line list can be used in the high temperature laboratory spectra analysis.

Inspection of Fig. 10 shows that, unusually, the maximum infrared absorption lies at 2.5 μm rather than at longer wavelengths. This is a manifestation of the unusual dipole

Table 10. $H_2{}^{32}S$ partition function values at different temperatures from different sources.

T	This work	HITRAN[a]	JPL[b]
2.725	1.0077		
5	1.2458		
9.375	2.9106		2.9106
18.75	8.6997		8.6996
37.5	23.8654		23.8654
75	65.5266	65.4854	65.5265
100	100.1557	99.97209	
150	182.7646	182.2696	182.7622
200	280.6278	279.6049	
225	334.6933	333.3219	334.5222
296	505.7921	503.07[c]	
300	516.1942	513.3829	514.4470
400	803.3417	797.6368	
500	1146.2892	1136.46	
600	1552.6512	1537.079	
700	2032.2186	2009.062	
800	2596.5908	2563.217	
900	3258.9381	3211.929	
1000	4033.8404	3968.802	
1100	4937.2034	4848.387	
1200	5986.2329	5866.361	
1300	7199.4423	7039.470	
1400	8596.6730	8385.471	
1500	10199.1148	9923.019	
1600	12029.3175	11672.66	
1700	14111.1872	13655.08	
1800	16469.9578	15893.10	
1900	19132.1349	18409.06	
2000	22125.4048	21229.28	

[a] As calculated using the HITRAN's FORTRAN programs for partition functions sums.
[b] As published on the JPL's website; values are very similar to those given by CDMS.
[c] From Šimečková et al. (2006).

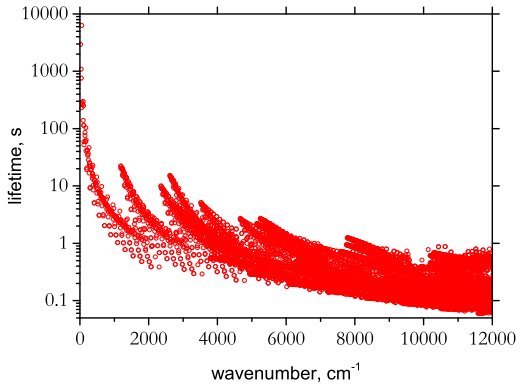

Figure 9. Lifetimes of H_2S obtained using the line list (ATY2).

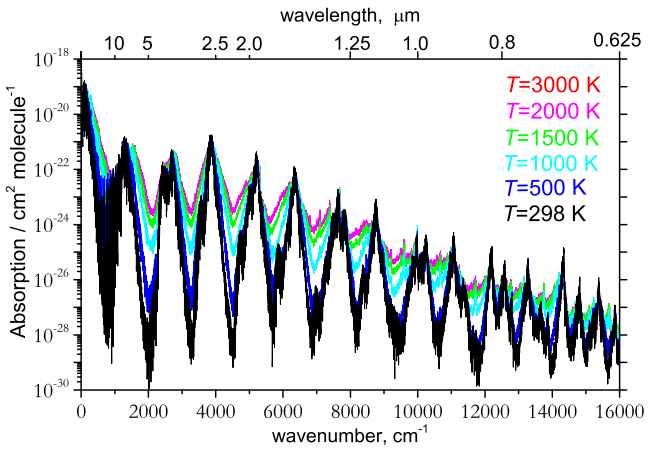

Figure 10. Temperature-dependent spectra generated using the ATY2 line list.

moment of H_2S which results in the fundamental bands being weaker than the overtones at about 2.5 μm.

6 CONCLUSION

A new hot line list for H_2S, called ATY2, has been computed containing 114 million transitions. The line list is divided into an energy file and a transitions file. This is done using the new ExoMol format (Tennyson et al. 2016a). The full line list can be downloaded from the CDS, via `ftp://cdsarc.u-strasbg.fr/pub/cats/J/MNRAS/xxx/yy`, or `http://cdsarc.u-strasbg.fr/viz-bin/qcat?J/MNRAS//xxx/yy`, as well as the ExoMol website, `www.exomol.com`. The line lists and partition function together with auxiliary data including the potential parameters and dipole moment functions, as well as the absorption spectrum given in cross section format (Hill et al. 2013), can all be obtained also from `www.exomol.com` as part of the extended ExoMol database (Tennyson et al. 2016a).

ACKNOWLEDGEMENTS

This work was supported by the ERC under the Advanced Investigator Project 267219 and the University of Jordan. JT and SNY thank the support of the COST action MOLIM (CM1405). We thank the Royal Society for supporting a visit by OVN to London.

REFERENCES

Aladro R., Martin S., Martin-Pintado J., Mauersberger R., Henkel C., Ocana Flaquer B., Amo-Baladron M. A., 2011, A&A, 535, A84
Azzam A. A. A., 2013, PhD thesis, University College London
Azzam A. A. A., Yurchenko S. N., Tennyson J., Martin M.-A., Pirali O., 2013, J. Quant. Spectrosc. Radiat. Transf., 130, 341
Azzam A. A. A., Lodi L., Yurchenko S. N., Tennyson J., 2015, J. Quant. Spectrosc. Radiat. Transf., 161, 41
Barber R. J., Tennyson J., Harris G. J., Tolchenov R. N., 2006, MNRAS, 368, 1087
Belov S. P., Yamada K. M. T., Winnewisser G., Poteau L., Bocquet R., Demaison J., Polyansky O., Tretyakov M. Y., 1995, J. Mol. Spectrosc., 173, 380
Biver N., et al., 2002, Earth Moon Planets, 90, 323
Bockelée-Morvan D., Colom P., Crovisier J., Despois D., Paubert G., 1991, Nature, 350, 318
Brown L. R., Crisp J. A., Crisp D., Naumenko O. V., Smirnov M. A., Sinitsa L. N., 1997, SPIE, 3090, 111
Brown L. R., Crisp J. A., Crisp D., Naumenko O. V., Smirnov M. A., Sinitsa L. N., Perrin A., 1998, J. Mol. Spectrosc., 188, 148
Brown L. R., o. v. Naumenk Polovtseva E. R., Sinitsa L. N., 2004a, 14th Symposium on High-Resolution Molecular Spectroscopy,, 5311, 59
Brown L. R., o. v. Naumenko Polovtseva E. R., Sinitsa L. N., 2004b, Eleventh International Symposium on Atmospheric and Ocean Optics/Atmospheric Physics, 5743, 1
Burenin A. V., Fevralskikh T. M., Melnikov A. A., Shapin S. M., 1985, J. Mol. Spectrosc., 109, 1
Burrus C. A., JR. Gordy W., 1953, Phys. Rev., 92, 274
Bykov A. D., Naumenko O. V., Smirnov M. A., Sinitsa L. N., Brown L. R., Crisp J., Crisp D., 1994, Can. J. Phys., 72, 989
Campargue A., Flaud J.-M., 1999, J. Mol. Spectrosc., 194, 43
Carleer M., et al., 1999, J. Chem. Phys., 111, 2444
Carvajal M., Lemus R., 2015, J. Phys. Chem. A, 119, 12823
Cazzoli, Gabriele Puzzarini, Cristina Gauss, Jürgen 2014, A&A, 566, A52
Cours T., Rosmus P., Tyuterev V. G., 2000, Chem. Phys. Lett., 331, 317
Cours T., Rosmus P., Tyuterev V. G., 2002, J. Chem. Phys., 117, 5192
Cupp R. E., Keikpf R. A., Gallagher J. J., 1968, Phys. Rev., 171, 60
Ding Y., Naumenko O., Hu S.-M., Zhu Q., Bertseva E., Campargue A., 2003, J. Mol. Spectrosc., 217, 222
Flaud J.-M., Camy-Peyret C., Johns J. W. C., 1983, Can. J. Phys., 61, 1462
Flaud J. M., Grosskloss R., Rai S. B., Struber R., Demtroder W., Tate D. A., guo Wang L., Gallagher T. F., 1995, J. Mol. Spectrosc., 172, 275
Flaud J.-M., Vaittinen O., Campargue A., 1998, J. Mol. Spectrosc., 190, 262
Gillis J. R., Edwards T. H., 1981, J. Mol. Spectrosc., 85, 55
Grosch H., Fateev A., Clausen S., 2015, J. Quant. Spectrosc. Radiat. Transf., 154, 28
Großkloß R., Rai S. B., Stuber R., Demtroder W., 1994, Chem. Phys. Lett., 229, 609
Helminger P., Cook R. L., De Lucia F. C., 1972, J. Chem. Phys., 56, 4581
Henon E., Cours T., Tyuterev V. G., 2003, Chem. Phys. Lett., 367, 284
Hill C., Yurchenko S. N., Tennyson J., 2013, Icarus, 226, 1673
Hoshyaripour G., Hort M., Langmann B., 2012, Geochem. Geophys. Geosys., 13, Q07004
Hu R., Seager S., Bains W., 2013, ApJ, 769
Huiszoon C., 1971, Rev. Sci. Instrum., 42, 477
Huiszoon C., Dymanus A., 1966, Phys. Lett., 21, 164
Jacquinet-Husson N., et al., 2011, J. Quant. Spectrosc. Radiat. Transf., 112, 2395
Jacquinet-Husson N., et al., 2016, J. Mol. Spectrosc.
Jensen P., 2012, WIREs Comput. Mol. Sci., 2, 494
Khayat A. S., Villanueva G. L., Mumma M. J., Tokunaga A. T., 2015, Icarus, 253, 130
Kyuberis A. A., Polyansky O. L., Lodi L., Tennyson J., Ovsyannikov R. I., Zobov N., 2016, MNRAS
Lane W. C., Edwards T. H., Gillis J. R., Bonomo F. S., Murcray

F. J., 1982, J. Mol. Spectrosc., 95, 365
Llavador Colomer F., Espinos Morato H., Mantilla Iglesias E., 2012, J. Air Waste Management Assoc., 62, 758
Lodi L., Tennyson J., 2010, J. Phys. B: At. Mol. Opt. Phys., 43, 133001
Lodi L., Tennyson J., 2012, J. Quant. Spectrosc. Radiat. Transf., 113, 850
Lynas-Gray A. E., Miller S., Tennyson J., 1995, J. Mol. Spectrosc., 169, 458
Miller R. E., Leroi G. E., Hard T. M., 1969, J. Chem. Phys., 50, 677
Miller S., Tennyson J., Rosmus P., Senekowitsch J., Mills I. M., 1990, J. Mol. Spectrosc., 143, 61
Müller H. S. P., Thorwirth S., Roth D. A., Winnewisser G., 2001, A&A, 370, L49
Müller H. S. P., Schlöder F., Stutzki J., Winnewisser G., 2005, J. Molec. Struct. (THEOCHEM), 742, 215
Naumenko O., Campargue A., 2001a, J. Mol. Spectrosc., 209, 242
Naumenko O., Campargue A., 2001b, J. Mol. Spectrosc., 210, 224
Neufeld, D. A. et al., 2015, A&A, 577, A49
Omont A., Lucas R., Morris M., Guilloteau S., 1993, A&A, 267, 490
Pickett H. M., Poynter R. L., Cohen E. A., Delitsky M. L., Pearson J. C., Muller H. S. P., 1998, J. Quant. Spectrosc. Radiat. Transf., 60, 883
Polovtseva E. R., Lavrentiev N. A., Voronina S. S., Naumenko O. V., Fazliev A. Z., 2012, Atmospheric and Oceanic Optics, 25, 157
Polyansky O. L., Bielska K., Ghysels M., Lodi L., Zobov N. F., Hodges J. T., Tennyson J., 2015, Phys. Rev. Lett., 114, 243001
Rothman L. S., et al., 2009, J. Quant. Spectrosc. Radiat. Transf., 110, 533
Rothman L. S., et al., 2013, J. Quant. Spectrosc. Radiat. Transf., 130, 4
Russell C. T., Kivelson M. G., 2001, J. Geophys. Res. Planets, 106, 33267
Seager S., Bains W., Hu R., 2013, ApJ, 775, 104
Senekowitsch J., Carter S., Zilch A., Werner H.-J., Handy N. C., 1989, J. Chem. Phys., 90, 783
Sharpe S. W., Johnson T. J., Sams R. L., Chu P. M., Rhoderick G. C., Johnson P. A., 2004, Appl. Spectrosc., 58, 1452
Šimečková M., Jacquemart D., Rothman L. S., Gamache R. R., Goldman A., 2006, J. Quant. Spectrosc. Radiat. Transf., 98, 130
Snyder L. E., Edwards T. H., 1969, J. Mol. Spectrosc., 31, 347
Strow L. L., 1983, J. Quant. Spectrosc. Radiat. Transf., 29, 395
Szabo A., Mohacsi A., Gulyas G., Bozoki Z., Szabo G., 2013, Meas. Sci. Technol., 24, 065501
Tarczay G., Császár A. G., Polyansky O. L., Tennyson J., 2001, J. Chem. Phys., 115, 1229
Tennyson J., 2012, WIREs Comput. Mol. Sci., 2, 698
Tennyson J., 2014, J. Mol. Spectrosc., 298, 1
Tennyson J., Sutcliffe B. T., 1986, Mol. Phys., 58, 1067
Tennyson J., Sutcliffe B. T., 1992, Intern. J. Quantum Chem., 42, 941
Tennyson J., Yurchenko S. N., 2012, MNRAS, 425, 21
Tennyson J., Kostin M. A., Barletta P., Harris G. J., Polyansky O. L., Ramanlal J., Zobov N. F., 2004, Comput. Phys. Commun., 163, 85
Tennyson J., Hulme K., Naim O. K., Yurchenko S. N., 2016b, J. Phys. B: At. Mol. Opt. Phys.
Tennyson J., Yurchenko S. N., The ExoMol team 2016a, J. Mol. Spectrosc.
Thaddeus P., Wilson R. W., Kutner M. L., Jefferts K. B., Penzias A. A., 1972, ApJ, 176, L73
Tyuterev V. G., Tashkun S. A., Schwenke D. W., 2001, Chem. Phys. Lett., 348, 223
Tyuterev V. G., Regalia-Jarlot L., Schwenke D. W., Tashkun S. A., Borkov Y. G., 2004, Comptes Rendus Physique, 5, 189
Ulenikov O. N., Malikova A. B., Koivusaari M., Alanko S., Anttila R., 1996a, J. Mol. Spectrosc., 176, 229
Ulenikov O. N., Onopenko G. A., Koivusaari M., Alanko S., Anttila R., 1996b, J. Mol. Spectrosc., 176, 236
Ulenikov O. N., Liu A.-W., Bekhtereva E. S., Gromova O. V., Hao L.-Y., Hu S.-M., 2004, J. Mol. Spectrosc., 226, 57
Ulenikov O. N., Liu A.-W., Bekhtereva E. S., Gromova O. V., Hao L.-Y., Hu S.-M., 2005, J. Mol. Spectrosc., 234, 270
Underwood D. S., Tennyson J., Yurchenko S. N., Huang X., Schwenke D. W., Lee T. J., Clausen S., Fateev A., 2016, MNRAS
Vaittinen O., Biennier L., Campargue A., Flaud J.-M., Halonen L., 1997, J. Mol. Spectrosc., 184, 288
Visscher C., Lodders K., Fegley Jr. B., 2006, A&A, 648, 1181
Von Zahn U., Moroz V. I., 1985, Adv. Space Res., 5, 173
Wakelam V., Castets A., Ceccarelli C., Lefloch B., Caux E., Pagani L., 2004, A&A, 413, 609
Werner H.-J., Knowles P. J., Knizia G., Manby F. R., Schütz M., 2012, WIREs Comput. Mol. Sci., 2, 242
Yamada K. M. T., Klee S., 1994, J. Mol. Spectrosc., 166, 395
Yurchenko S. N., Thiel W., Jensen P., 2007, J. Mol. Spectrosc., 245, 126
Zahnle K., Marley M. S., Freedman R. S., Lodders K., Fortney J. J., 2009, ApJ, 701, L20
Zak E., Tennyson J., Polyansky O. L., Lodi L., Tashkun S. A., Perevalov V. I., 2016, J. Quant. Spectrosc. Radiat. Transf.
de Bergh C., Moroz V. I., Taylor F. W., Crisp D., Bézard B., Zasova L. V., 2006, Planet Space Sci., 54, 1389

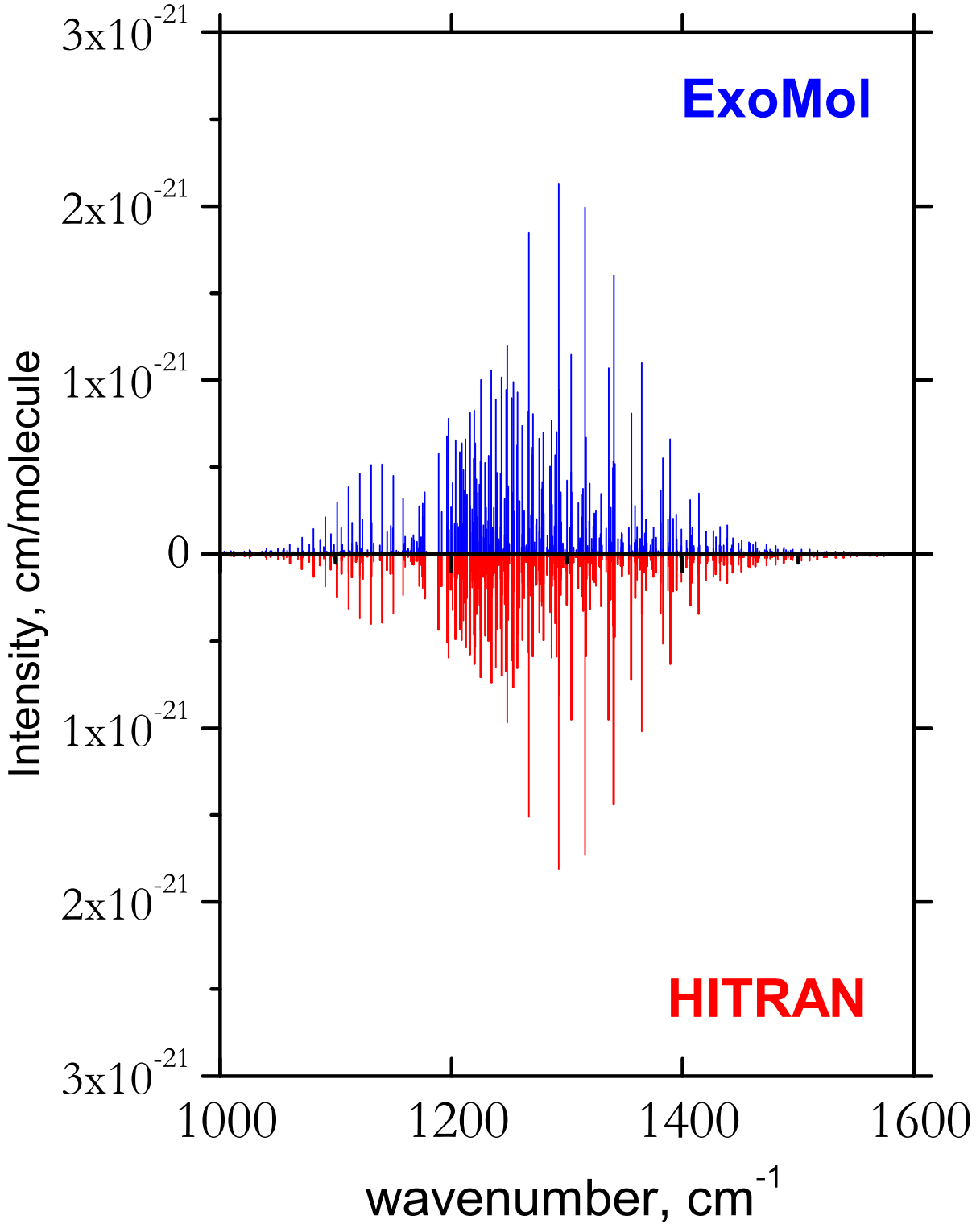
ExoMol
HITRAN
3x10-21
2x10-21
1x10-21
0
1x10-21
2x10-21
3x10-21
1000
1200
1400
1600
Intensity, cm/molecule
wavenumber, cm-1